Hindawi
Geofluids
Volume 2020, Article ID 8854545, 17 pages
https://doi.org/10.1155/2020/8854545

Research Article

A New Methodology for the Multilayer Tight Oil Reservoir Water Injection Efficiency Evaluation and Real-Time Optimization

Lin Cao,[1,2] Jianlong Xiu,[3] Hongjie Cheng,[4] Hui Wang,[5] Shujian Xie,[6] Hui Zhao,[6] and Guanglong Sheng[6]

[1]*School of Engineering Science, University of Chinese Academy of Sciences, Beijing 100049, China*
[2]*Institute of Porous Flow & Fluid Mechanics, Chinese Academy of Sciences, Langfang 065007, China*
[3]*PetroChina Research Institute of Petroleum Exploration & Development, Beijing 100083, China*
[4]*Exploitation and Development Research Institute, PetroChina Xinjiang Oilfield Company, Karamay, Xinjiang 834000, China*
[5]*The No. 2 Oil Production Plant, PetroChina Xinjiang Oilfield Company, Karamay, Xinjiang 834000, China*
[6]*College of Petroleum Engineering, Yangtze University, Wuhan, Hubei 430100, China*

Correspondence should be addressed to Jianlong Xiu; xiujianlong69@petrochina.com.cn

Received 10 June 2020; Revised 20 August 2020; Accepted 21 August 2020; Published 10 November 2020

Academic Editor: Wei Wei

It is important to determine the reasonable injection and production rates in the development of multilayer tight oil reservoir with water flooding treatment. Based on the INSIM (interconnection-based numeric simulation model), a connected network model, a new method is designed to evaluate the water injection efficiency of different layers in water flooding reservoirs and to optimize the injection-production system to produce more oil. Based on the types of sedimentary facies and corresponding injection-production data, the interwell connections are divided into four major categories (middle channel, channel edge, middle channel bar, and channel bar edge) and twelve subclasses. This classification standard of interwell connections could help to significantly improve the accuracy of judging the dominant flow path without constructing a complicated geological model. The interaction of interwells such as injection-production correlation and water injection efficiency could be revealed by simulating the production performance and computing the layer dividing coefficient and well dividing coefficient. A numerical example is used to validate this method by comparing results from FrontSim and this method, and the computational efficiency of this method is several dozen times faster than that of the traditional numerical simulation. This method is applied to quickly optimize the production schedule of a tight oil reservoir with the water flooding treatment, that is, the water injection rate of multilayer reservoirs could be optimized subtly by the injection efficiency of different layers, and the target of producing more oil with lower water cut could be achieved.

1. Introduction

Waterflooding operations are performed to improve the oil recovery of reservoirs worldwide [1]. In some oil fields with many wells and a long production history, the wide expansion of the injection water and the continuous changes in the flow field in the layer results in water channeling and dead oil areas [2, 3]. These problems are mainly due to two factors. First, the physical properties of the reservoir are affected by the sedimentary environment, tectonic movement, and diagenesis; there are intralayer and interlayer heterogeneities in the reservoir. Second, unreasonable injection and production systems have exacerbated the phenomenon of injection water fingering and bottom water coning. Therefore, based on the existing reservoir development knowledge, it is important to identify the injection-production correspondence, to accurately determine the dominant flow path, and to evaluate the injection efficiency of the injectors [4, 5]. This forms both the key issue and the basic work to increase the high economic value oil production and to determine a reasonable injection-production system [6, 7].

Due to the relatively poor physical properties of tight oil reservoirs, the following measures were used to optimize

the development effect currently, including fracturing [8], asynchronous injection alternating production [9], water flooding huff-puff of horizontal wells [10], and CO_2 huff and puff of horizontal wells [11]. Flow paths can reflect the flow behavior of fluid in a period of time, so it is often used to evaluate the development effect of reservoir under a certain working system. Commonly used methods for distinguishing flow paths include the tracer method, reservoir numerical simulations [12–14], and data-driven models. The tracer test incurs significant time to acquire results, and some operations during the test have a certain impact on the normal reservoir production. In multilayer waterflooding reservoir, the capillary forces may have a significant effect to change the flow pathways [15]. Therefore, although this method has high accuracy, it is difficult to popularize and to apply on a large scale in a reservoir. Reservoir numerical simulation methods are restricted by model accuracy, and it is difficult to achieve accurate real-time analysis of the entire reservoir. Data-driven models, as part of a new class of dominant flow path identification methods, do not require complex geological modeling and can determine information such as fluid flow dynamics and water injection efficiency through the analysis of the production data. There are currently two kinds of data-driven models, namely, the CRM (capacitance-resistive model) and the INSIM (interconnection-based numeric simulation model). The CRM was first used by Yousef et al. [16] to determine the connectivity between wells in 2005. Following that, the model was used in waterflooding reservoirs [17], large-scale reservoirs [18], and analysis of the formation damage from injected water [19]. Zhao et al. [20] proposed the INSIM in 2015. By simplifying the characterization of the reservoir as a network of interconnected nodes that consider a series of complex geological features such as wells, water bodies, and faults, an interwell connection network is established. It is characterized by two parameters, connected volume and transmissibility, to fit the actual production dynamics, to correct the interwell connection parameters, and to make the model conform to the actual connectivity of the reservoir. Because a complex geological modeling process is not considered, the INSIM and its derived INSIM-FT (interconnection-based numeric simulation model with front-tracking algorithm) [21–22] and INSIM-FPT (interconnection-based numeric simulation model with the flow-path tracking strategy) [23] reduce the modeling time significantly, while considering reservoir properties and maintaining the calculation accuracy. Based on the distribution of sedimentary facies in each layer, this study identifies the influence of different sedimentary environments on the interwell connection relationship of INSIM. The pressure, saturation, and water cut of each node are solved by the connection parameters corrected by production data combined with the principle of material balance. Then, the vertical/plane dividing coefficient and water injection efficiency of the injector are obtained. Based on this, the water injection efficiency of each layer is calculated and combined by the optimization principle to optimize the injection and production systems [24, 25].

Since the main factors affecting the accuracy of the water injection efficiency evaluation method are INSIM's modeling data and the model's historical fitting results, the method has good general applicability to the reservoirs applicable to INSIM. At present, the INSIM model has been widely used in sand reservoirs, carbonate reservoirs, fracture-cavity reservoirs, etc. This method has certain practical significance for evaluating the water injection efficiency of these types of reservoirs. Compared with the traditional reservoir numerical simulation method [26, 27], the calculation speed of the water injection efficiency is significantly improved. It is of great significance to accurately identify the injection-production correspondence relationship and increase oil production at a lower cost.

2. Water Injection Efficiency Evaluation Method and Optimization Theory

2.1. The Calculation of Water Injection Dividing Coefficient Based on INSIM. The interwell connection unit constructed by the INSIM model contains two characterization parameters: transmissibility and connection volume. Transmissibility represents the flow capacity of formation fluids in units under unit pressure difference, which is mainly affected by permeability and fluid properties. Connection volume reflects the material basis of units, mainly related to well spacing, effective thickness, and porosity of the reservoir. After establishing the INSIM (Figure 1), the material balance equation of the fluid in the connected unit can be obtained by

$$\sum_{k=1}^{N_l}\sum_{j=1}^{N_w} T_{ijk}(t)\left(p_j(t)-p_i(t)\right)+q_i(t)=\frac{1}{2}\frac{dp_i(t)}{\mathrm{d}t}\sum_{k=1}^{N_l} C_{tk}\sum_{j=1}^{N_w} V_{ijk}(t). \tag{1}$$

The implicit difference discretization of Equation (1) can solve the bottom hole pressure of each well, then saturation and water cut of each node in the connected network can be calculated with the saturation-tracking method. Fitting the actual production data to correct the connection parameters is conducted to align the production result of the model with the actual production. Let the feature parameter matrix b denote the reservoir connectivity parameter, applying the stochastic perturbation approximate gradient algorithm (SPSA) to optimize the objective function $O(b)$ causes it to have a minimum value.

$$O(b)=\frac{1}{2}(b-b_r)^T G_B^{-1}(b-b_r)+\frac{1}{2}[k_{\mathrm{obs}}-h(b)]^T G_D^{-1}[k_{\mathrm{obs}}-h(b)]\,(b\geq 0). \tag{2}$$

Using percolation theory and interwell connection parameters, the production index in the cross-well connectivity unit can be expressed as

$$J_{ijk}^n=\frac{4T_{ijk}^n\lambda_{ik}^{n-1}}{\lambda_{ijk}^{n-1}\left[\ln\left(0.5L_{ijk}/r_{ik}\right)+s_{ik}-0.75\right]}. \tag{3}$$

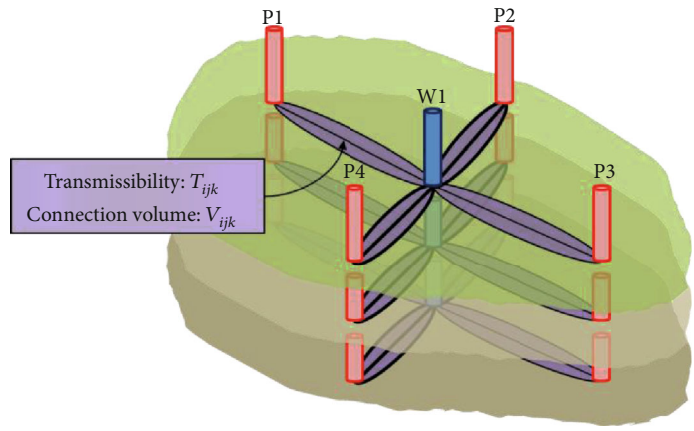

Figure 1: A sketch map of the INSIM in a multilayer reservoir.

Combining the bottom hole pressure and the production index, the phase mobility in the connected unit is determined by the upstream weight method:

$$\lambda_{ijk}^{n} = \begin{cases} \lambda_{ik}^{n-1} = K_{ijk}\left[\dfrac{K_{ro}\left(S_{wik}^{n-1}\right)}{\mu_{ok}} + \dfrac{K_{rw}\left(S_{wik}^{n-1}\right)}{\mu_{wk}}\right] & p_i^{n-1} \geq p_j^{n-1}, \\ \lambda_{jk}^{n-1} = K_{ijk}\left[\dfrac{K_{ro}\left(S_{wik}^{n-1}\right)}{\mu_{ok}} + \dfrac{K_{rw}\left(S_{wik}^{n-1}\right)}{\mu_{wk}}\right] & p_i^{n-1} < p_j^{n-1}. \end{cases} \tag{4}$$

Based on the above method, the total production index of well i can be determined:

$$J_i^n = \sum_{k=1}^{N_l}\sum_{j=1}^{N_w} J_{ijk.}^n \tag{5}$$

Therefore, the vertical dividing coefficient of well i in layer k is determined by the ratio of the sum of the production index of well i in layer k to the total production index of well i:

$$A_{ik}^n = \frac{J_{ik}^n}{J_i^n} = \frac{\sum_{j=1}^{N_w} J_{ijk}^n}{\sum_{k=1}^{N_l}\sum_{j=1}^{N_w} J_{ijk}^n}. \tag{6}$$

Meanwhile, the plane dividing the coefficient between wells i and j is determined by the transmissibility between the nodes and the pressure difference:

$$A_{ijk}^n = \frac{q_{ijk}^n}{q_{ik}^n} = \frac{T_{ijk}^n\left(p_j^n - p_i^n\right)}{\sum_{j=1}^{N_w} T_{ijk}^n\left(p_j^n - p_i^n\right)}. \tag{7}$$

Compared to the dividing coefficient calculation method proposed in this study, the reservoir engineering method does not consider changes in pressure and uses only the percolation theory to calculate the dividing coefficient from the well properties.

$$A_{ik}^n = \frac{\sum_{j=1}^{N_w}\left(\overline{K_{ij}}\bullet\overline{h_{ij}}/L_{ij}\right)}{\sum_{k=1}^{N_l}\sum_{j=1}^{N_w}\left(\overline{K_{ij}}\bullet\overline{h_{ij}}/L_{ij}\right)}, \tag{8}$$

$$A_{ijk}^n = \frac{\overline{K_{ij}}\bullet\overline{h_{ij}}/L_{ij}}{\sum_{j=1}^{N_w}\left(\overline{K_{ij}}\bullet\overline{h_{ij}}/L_{ij}\right)}. \tag{9}$$

2.2. Water Injection Efficiency Calculation and Optimization. After clarifying the dividing coefficient in each layer, the layered water injection efficiency of the injectors can be solved further, that is, the ratio of the amount of oil displaced by the injector to the surrounding producers in this layer and the water injection amount of this layer. The ratio of the total oil production of layer k to the total water injection of layer k is the average water injection efficiency of layer k and is expressed as

$$e_{ik}^n = \frac{\sum_{j=1}^{N_w} q_{ik}^n A_{ijk}^n\left(1 - f_{wjk}^n\right)}{q_{ik}^n}, \tag{10}$$

$$e_{xk}^n = \frac{\sum_{i=1}^{N_I}\sum_{j=1}^{N_w} q_{ik}^n A_{ijk}^n\left(1 - f_{wjk}^n\right)}{\sum_{i=1}^{N_I} q_{ik}^n}. \tag{11}$$

After obtaining the water injection efficiency of each well in this layer, it should be compared with the average water injection efficiency of this layer to determine the liquid volume adjustment measures. When the water injection efficiency is higher than the average, the injection is increased; otherwise, the injection is reduced, and the liquid volume of each well in this layer is determined by Equations (12) and (13).

$$q_{ik}^{n+1} = q_{ik}^n(1 + \eta_i), \tag{12}$$

$$\eta_i = \begin{cases} \eta_{\max}\left(\dfrac{e_{ik}^n - e_{xk}^n}{e_{\max}^n - e_{xk}^n}\right)^{\alpha}, e_{ik}^n < e_{xk}^n, \\ \eta_{\min}\left(\dfrac{e_{xk}^n - e_{ik}^n}{e_{xk}^n - e_{\min}^n}\right)^{\alpha}, e_{ik}^n > e_{xk}^n. \end{cases} \tag{13}$$

In Equation (13), $\eta_{\max}$ and $\eta_{\min}$ are assigned to the values of -0.5 and 0.5, respectively. Because the fractional part value is less than or equal to 1, it means that the liquid volume adjustment range for the next time step will not be greater than 50% of the liquid volume in the previous time step. As the injection volume of the reservoir will not change significantly in a short time, to keep the injection volume of the entire reservoir constant, it is necessary to adjust the injection volume of each layer according to Equation (14). The well water injection volume is equal to the sum of the injection volume of each layer, as shown in Equation (15).

$$q_{ik}^{(n+1)} = \frac{\sum_{i=1}^{N_I}\sum_{k=1}^{N_l} q_{ik}^n}{\sum_{i=1}^{N_I}\sum_{k=1}^{N_l} q_{ik}^{n+1}} q_{ik}^{n+1}, \tag{14}$$

$$q_i^{n+1} = \sum_{k=1}^{N_l} q_{ik}^{n+1}. \tag{15}$$

After determining the liquid volume adjustment of the injectors, assuming that the reservoir injection-production ratio in the optimization stage is constant, the liquid volume adjustment of the production well is calculated from the injection volume and the dividing coefficient, as shown in Equation (16).

$$q_j^{n+1} = q_j^n + \sum_{i=1}^{N_{Ic}}\sum_{k=1}^{N_l} q_{ik}^{(n+1)} A_{ijk}^n. \tag{16}$$

3. The Conceptual Model

A two-layer model including five injectors and four producers is established to introduce the basic parameters of the INSIM and the workflow for calculating injection efficiency (IE). The producer-injector spacing is 200 m, and the thickness of each layer is 10 m. The range of permeability is 165.0 mD in the 1st layer and 171.6 mD in the 2nd layer, while the permeability field is shown in Figure 2. The initial oil saturation is 0.8. The viscosity of the formation water is 1.0 mPa s and the viscosity ratio of oil to water is 20. The daily water injection rate of each injector is 40 m^3/d. Before 3000 days, the daily fluid production rate of each producers is 50 m^3/d. From 3000–6000 days, the working system from P1 to P4 changes to 80 m^3/d, 60 m^3/d, 40 m^3/d, and 20 m^3/d, respectively, and the FrontSim streamline field is shown in Figure 3.

The initial value of the interwell connection parameters could be calculated from the well property data. Then, using the reservoir production data combined with the optimization theory, the initial value of the interwell connection parameters is corrected after the fitting indicators meet accuracy requirements. The final value of the interwell connection parameters is shown in Figure 4. The line between the wells shows the transmissibility of the reservoir; the red line indicates strong connectivity, the blue line indicates the second strongest connectivity, and the black line indicates weak connectivity. Upon comparing the distribution of strong connectivity with high permeability zones, these were found to be consistent. It shows that after correction, an INSIM could accurately characterize the reservoir properties and provide a reliable basis for calculating the dividing coefficient of injection water and evaluating the water injection efficiency.

In this study (Equation (6)), the reservoir engineering method (Equation (8)) and the streamline numerical simulation method are used to calculate the vertical dividing coefficient of each layer. Figures 5 and 6 show the difference between the calculation results of the INSIM method and other methods. From the result shown in Figure 6, the vertical dividing coefficient of the reservoir engineering method does not change because it does not consider the flow field change caused by the adjustment of the production system. However, the dominant seepage channel in the reservoir forms gradually and stabilizes with the development. Due to a superior physical property of the first layer in the model, the vertical dividing coefficient of the first layer gradually increases during the formation of the dominant seepage channel. Following the stabilization of the seepage channel, the vertical dividing coefficient also stabilizes. The method in this study and the streamline numerical method can reflect this law accurately.

Meanwhile, Equations (7) and (9) were used to calculate the plane dividing coefficient of the injection well at 6000 days. As shown in Figure 7, the plane dividing coefficient obtained based on this method is basically consistent with the results based on the streamline simulation, which verifies the reliability of this method. The reservoir engineering method cannot accurately reflect the plane dividing coefficient currently because it does not consider the changes in the reservoir production system. The streamline simulation method takes 25.54 seconds for one complete calculation. Compared to this method, the method in this study takes only 0.74 seconds for one complete calculation, which is faster by a factor of 35.

The single-well water injection efficiencies and average water injection efficiencies of the reservoir engineering method, streamline method, and method of this study are calculated using Equations (10) and (11), as shown in Figure 8. According to the reservoir engineering method, the water injection efficiency of each well is lower than the other two methods. Due to changes in the flow field, the division of injected water in each direction is different periodically. Some remaining oil is produced by adjusting the working system, and this volume of oil cannot be calculated using the reservoir engineering method. The method in this study solves this problem better by considering the change in the bottom hole pressure of each well, and the calculation results are basically consistent with the streamline method. By using the dividing coefficient and the water injection efficiency of the conceptual model in Equations (12), (13), (14), (15) and (16), the production system of each well in the optimization stage is calculated.

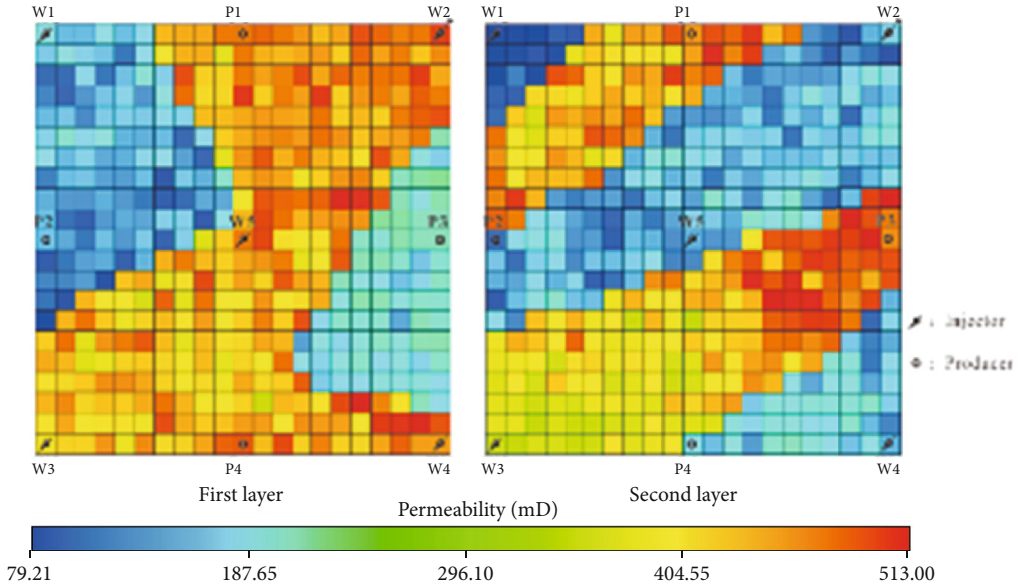

Figure 2: Model permeability field.

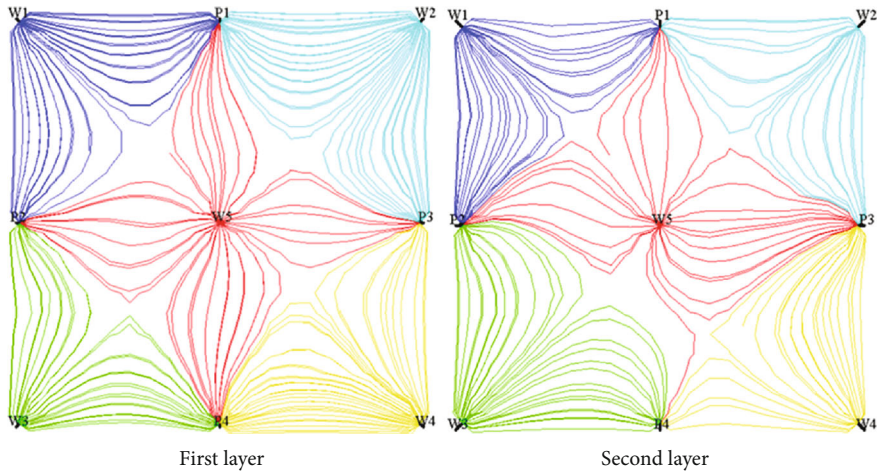

Figure 3: Streamline field in FrontSim.

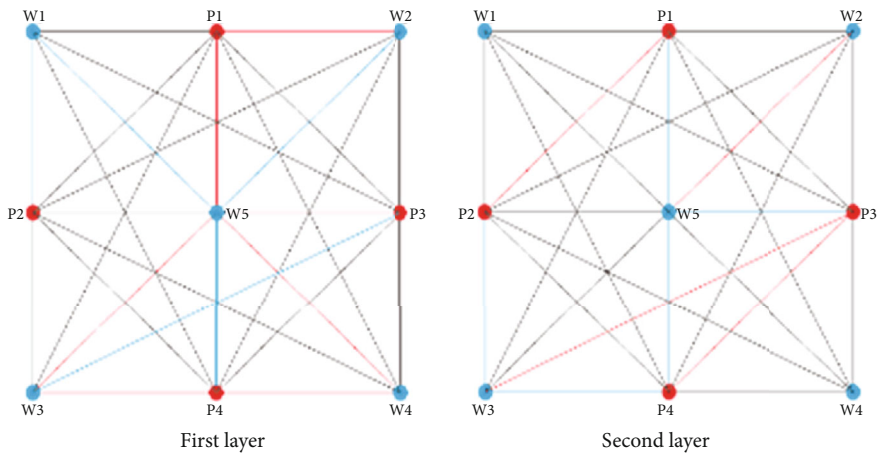

Figure 4: Model interwell connectivity field.

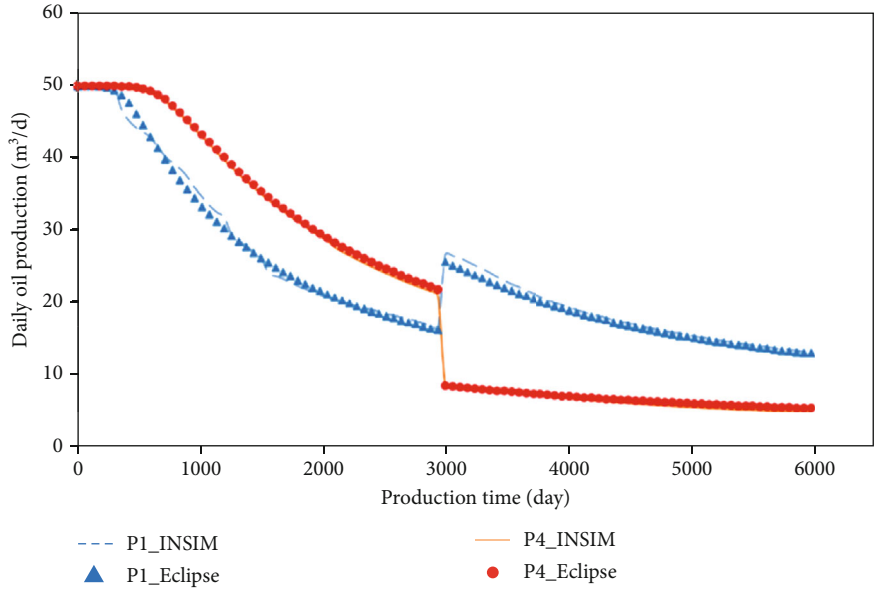

Figure 5: The fitting effect of daily oil production.

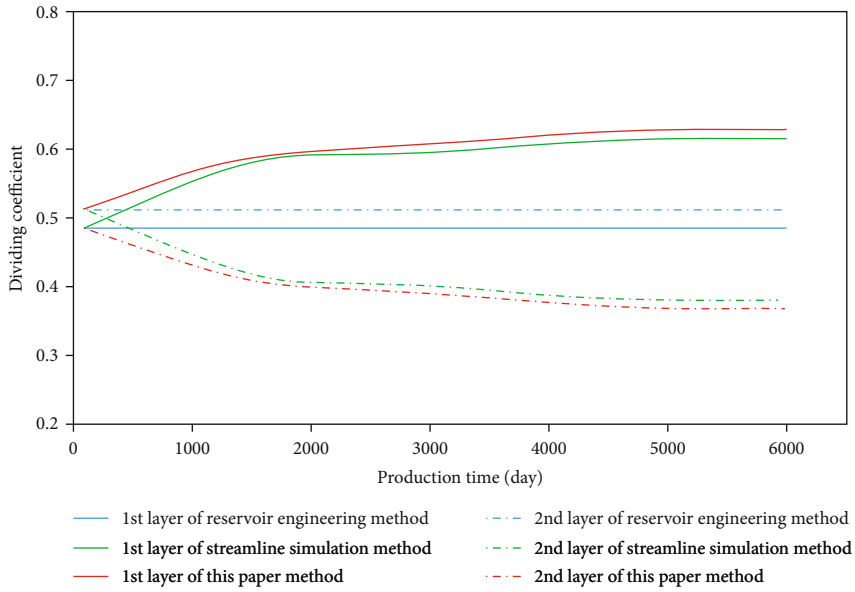

Figure 6: Vertical dividing coefficient of W5.

The production system of the original plan and the adjusted plan were brought into the Eclipse model to predict the oil production and the water cut of the reservoir after the implementation of the plan. As shown in Figure 9, five months after the implementation of the adjusted plan, the daily oil production of reservoir is increased, the comprehensive water cut of reservoir is decreased, and the adjusted plan had an optimized effect on the overall reservoir development.

4. Practical Applications

4.1. The Characterization of the Interwell Connection and the Evaluation of the Water Injection Efficiency. For the characterization, the layered water injection efficiency evaluation method based on the INSIM was applied to a tight oil reservoir. The adjustments to the production system proposed in this method were implemented in the field, which achieved good development results. This tight oil reservoir is an edge water reservoir controlled by structural lithology. It has an oil-bearing area of 9.3 km^2 and an effective thickness of 26.3 m. The reservoir is divided into upper sandstone sections and lower conglomerate sections; a separated waterflooding and comingled producing technology is used between different rock sections. The average porosity of the reservoir was 16.9%, the average permeability was 182.27×10^{-3} μm^2, the central reservoir depth was 1650 m, and the geological reserves were 1530.70×10^4 t. Since entering the

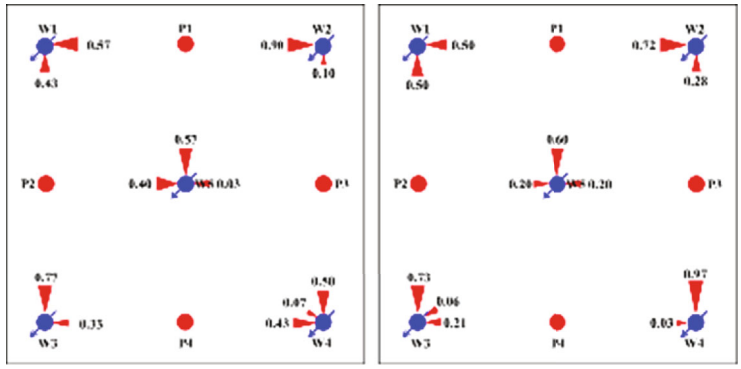

(a) Streamline simulation method

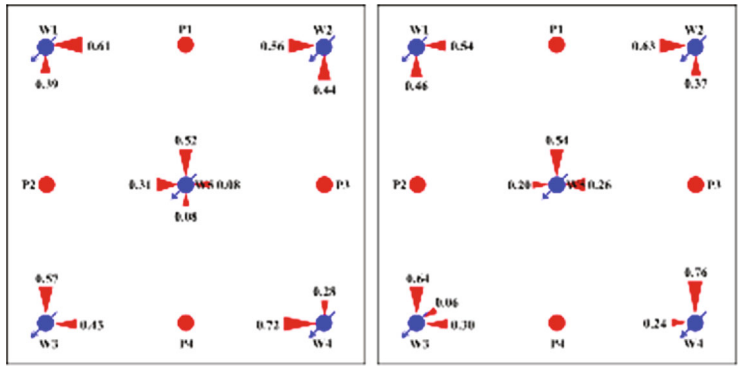

(b) Method in this study

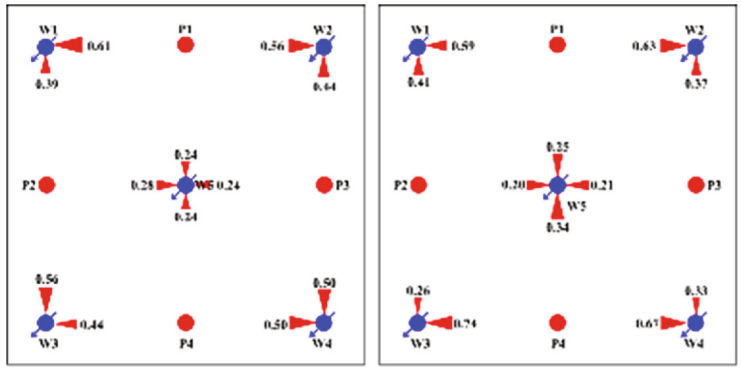

(c) Reservoir engineering method

Figure 7: The plane dividing coefficient of injectors in 6000 d.

second development stage in 2016, a total of 213 new wells were deployed, accessing geological reserves of 1105.43×10^4 t, and the average well spacing was reduced to 150 m. At the end of June 2018, 96 water injection wells and 133 oil wells were opened. The daily liquid production was 2837 t, the daily oil production was 370 t, and the comprehensive water cut was 86.9%. The recycle of injection water is inefficient in such a high water cut reservoir.

After history matching the INSIM (Figure 10), the field interwell connection obtained by fitting the production dynamics is shown in Figure 11, in which the red line represents a strong connectivity, the green line represents the second strongest connectivity, and the black line represents weak connectivity.

Based on the sedimentary facies' types of reservoirs and the INSIM, an interwell connectivity classification standard is established, which reflects the similarities and differences in the various sedimentary facies. The orange area represents the channel bar, and the light yellow and bright yellow areas represent the river channels, as shown in Figure 12. Overall, the connectivity from sandstone to conglomerate in the vertical direction deteriorates, and the permeability decreases. In

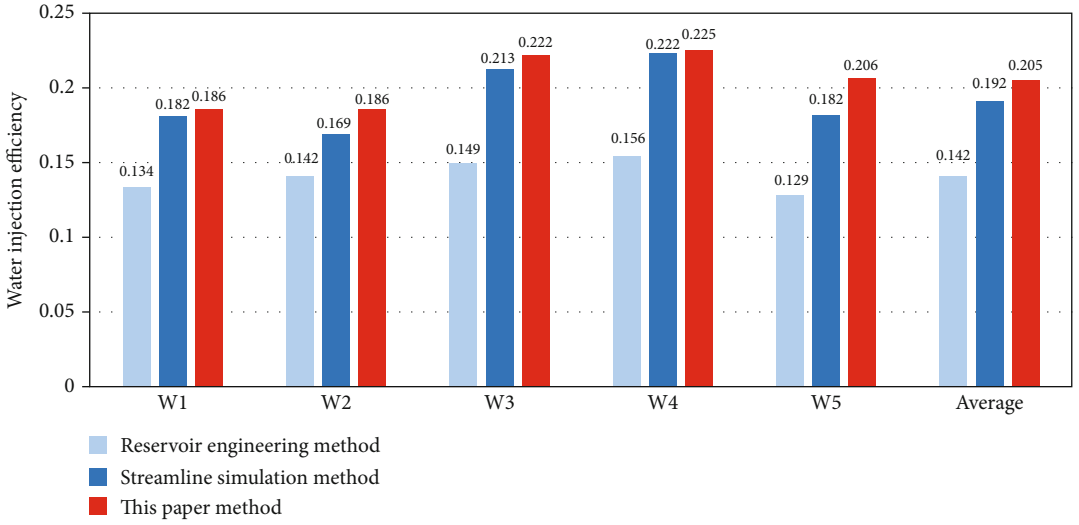

(a) The first layer

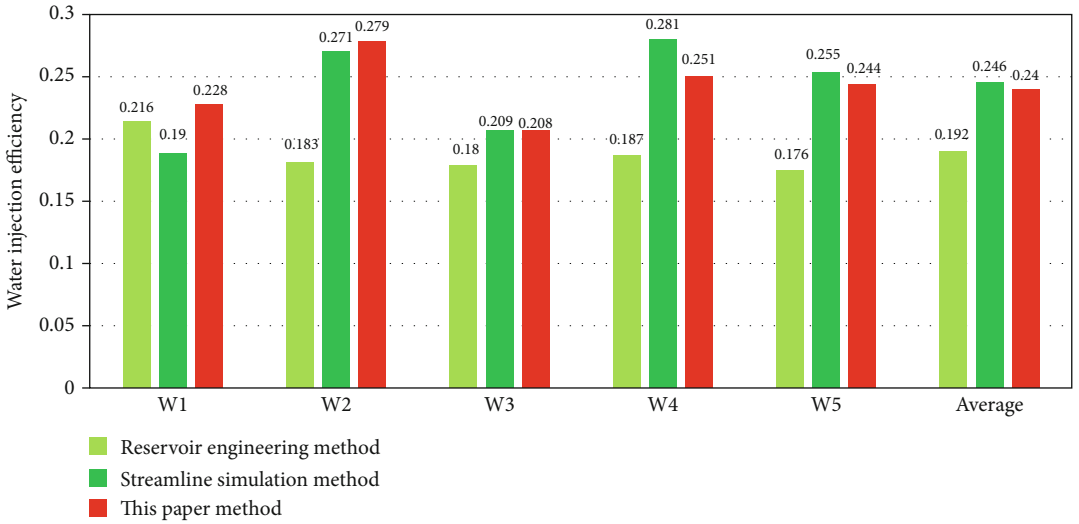

(b) The second layer

Figure 8: The water injection efficiency of injectors in three different methods.

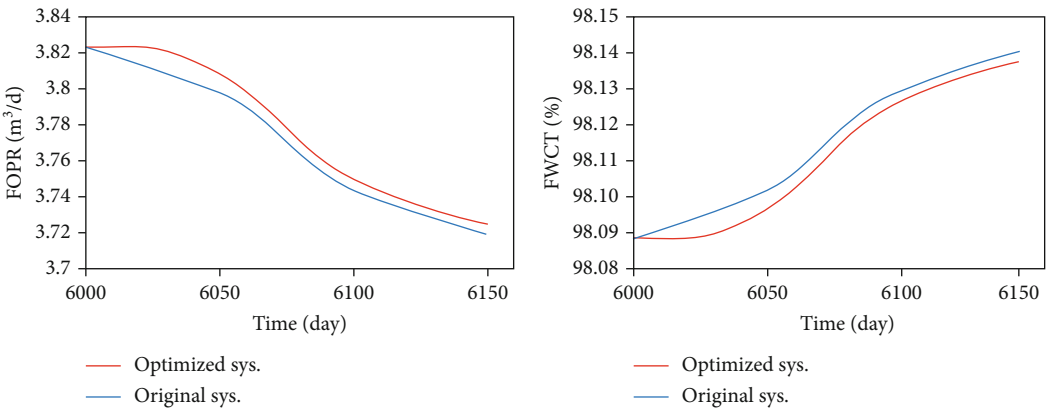

(a) Field oil production rate (FOPR)

(b) Field water cut (FWCT)

Figure 9: The comparison of optimized and original production systems.

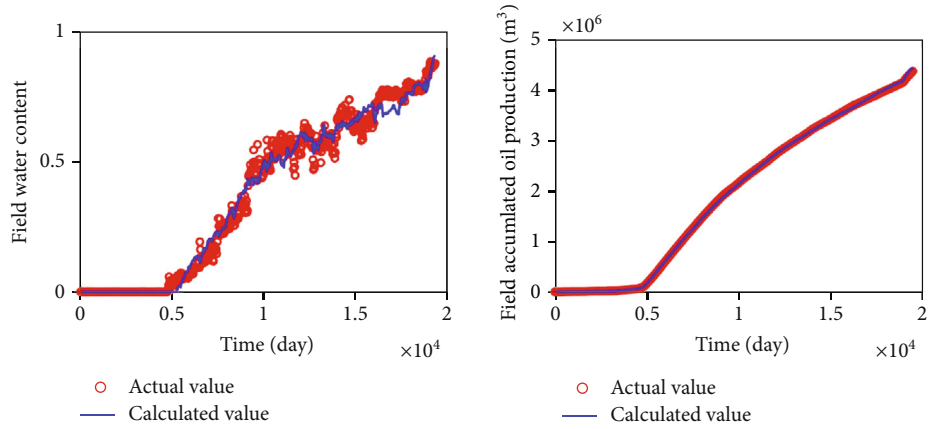

Figure 10: History matching results of the field water cut and total field oil production.

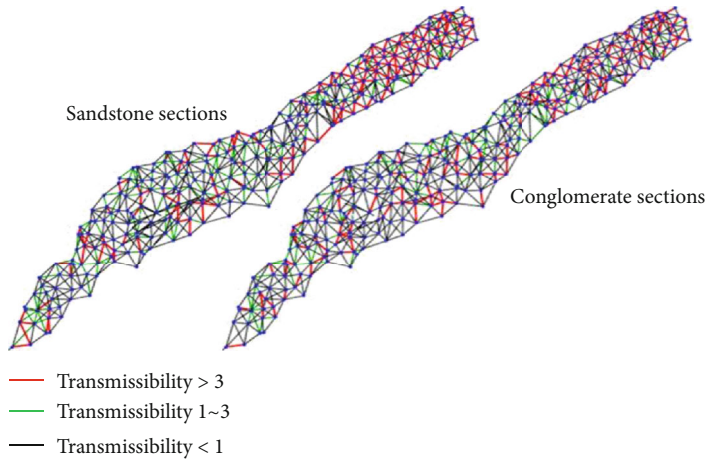

Figure 11: Reservoir interwell connectivity field.

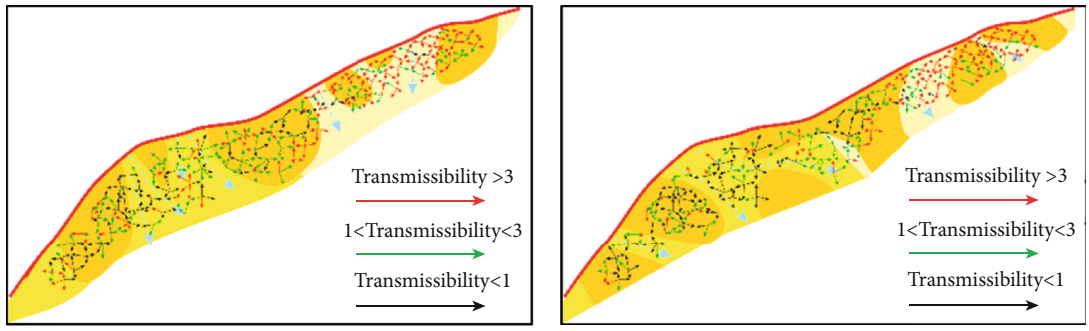

(a) Sandstone sections (b) Conglomerate sections

Figure 12: Interwell connectivity and sedimentary facies.

the plane, affected by source direction, the interwell connectivity from the southwest to the northeast improves and the permeability increases.

Combining the interwell connectivity with the sedimentary facies at the well nodes, the distribution pattern of the characteristics is obtained as shown in Table 1, which divides the interwell connectivity into four major categories and twelve subcategories. The four types include the middle channel, the side of channel, the middle of the channel bar, and the side of the channel bar. Since the porosity of different sedimentary facies of the same section in this tight oil reservoir is not much different, the connection volume is mainly affected by the well spacing, and different types of connection units cannot be accurately distinguished. Therefore, when

Table 1: The interwell connection structure pattern.

Categories	Types	Connection types	Structure	Transmissibility
Channel	Middle	Strong connection	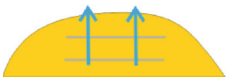	>3
		Medium-strength connection	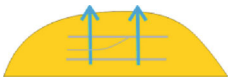	1 ~ 3
		Weak connection	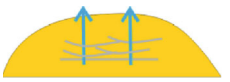	<1
			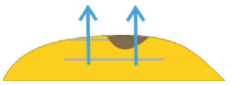	<1
	Side	Strong connection	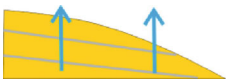	>3
		Medium-strength connection	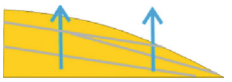	1–3
		Weak connection	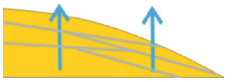	<1
Channel bar	Middle	Strong connection	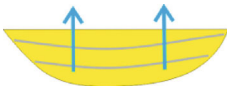	>3
				>3
		Medium-strength connection	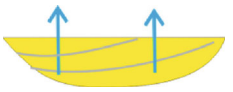	1–3
		Weak connection	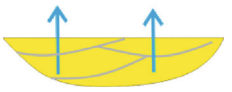	<1
	Side	Strong connection		>3
		Medium-strength connection	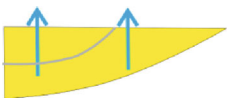	1–3
		Weak connection	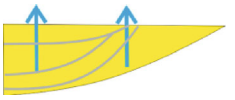	<1
Channel-channel bar		Medium-strength connection		1–3
		Weak connection	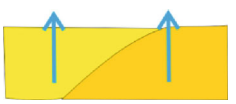	<1

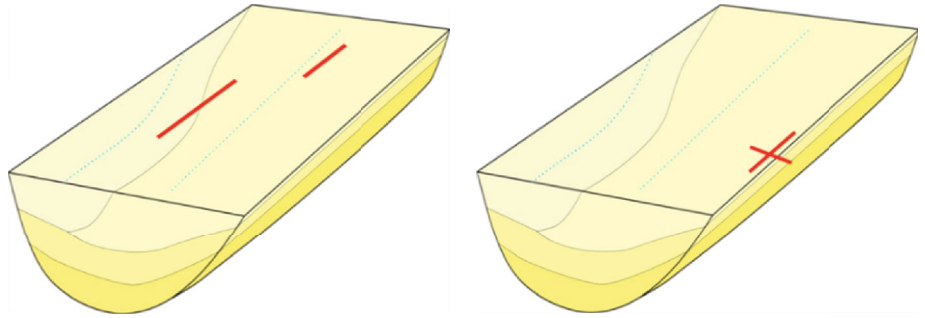

(a) Middle of channel (b) Side of channel

Figure 13: Channel sedimentary structure.

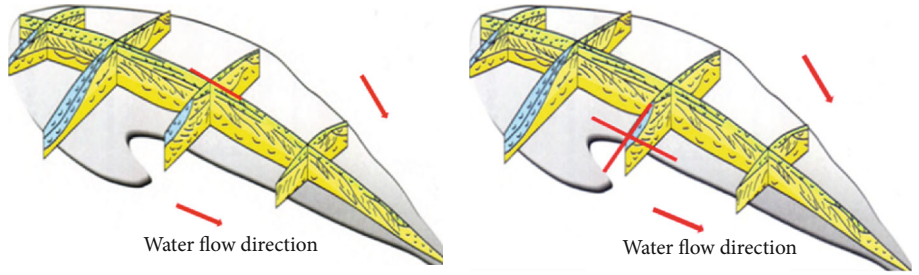

(a) Middle of the channel bar (b) Side of the channel bar

Figure 14: Channel bar sedimentary structure.

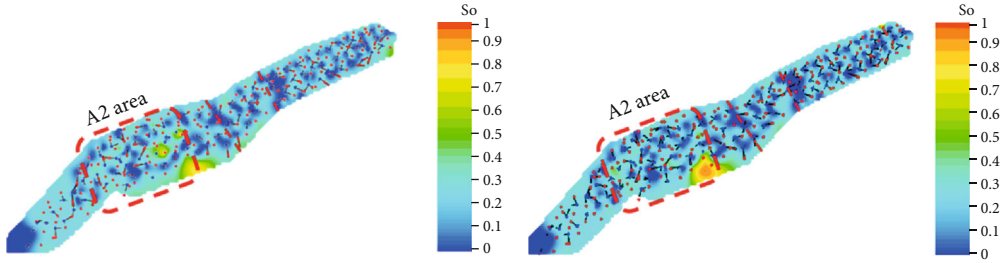

(a) Sandstone sections (b) Conglomerate sections

Figure 15: Oil saturation field.

dividing the types of interwell connection units, only choose the transmissibility and divide it into three types as the criteria for connectivity classification. The three types of connectivity classification include $T_{ij} > 3$, $1 < T_{ij} < 3$, and $T_{ij} < 1$, which, respectively, indicate strong, medium, and weak connectivity of the interwell transmissibility based on the proportion of each subtype in the different types of sedimentary facies. In the middle channel, the interwell is well connected and exhibits anisotropy. In the side of the channel, the interwell has a partial connection, with significant anisotropy. In the middle of the channel bar, the interwell is connected, and there is a large difference between the channel bars. In the side of the channel bar, the interwell is connected in some directions, and the physical properties are relatively worse.

The sedimentary structure of the middle channel is shown in Figure 13(a). The middle channel has a thick channel sediment with good properties. When the two wells are connected parallel to the source direction, the connectivity between the wells is good and may develop a dominant seepage channel. As shown in Figure 13(b), the sedimentary period changes quickly to the side of the channel and the sediment thickness of a single period decreases. Correspondingly, the flow barriers between sand bodies are more developed. Furthermore, the flow barriers cause the properties of the reservoir to become worse than those of the middle channel. The interwell connectivity is without change, and the dominant seepage channel is infrequent. In general, the connectivity of the parallel source direction is better than that of the vertical source direction.

As shown in Figure 14(a), the central area of the channel bar is dominated by parallel interlayers. The parallel interlayers of sand bodies between wells in the central area are uniformly distributed, with good connectivity in all directions. Additionally, the dominant seepage channels are developed.

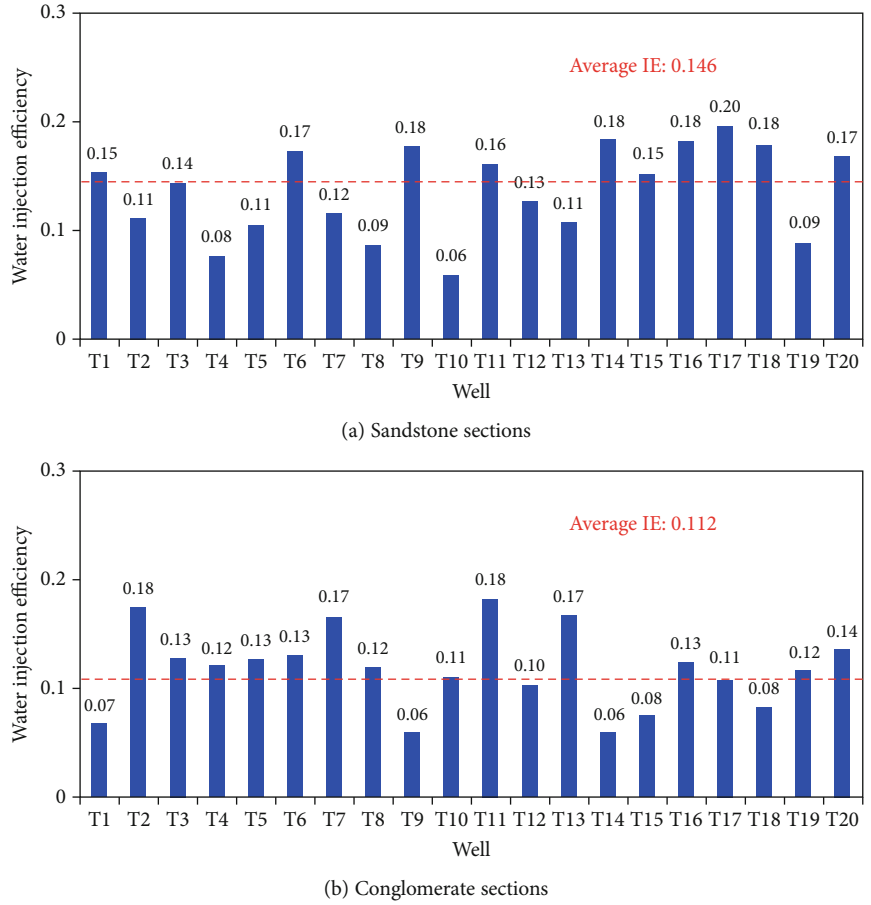

(a) Sandstone sections

(b) Conglomerate sections

Figure 16: Water injection efficiency of injectors.

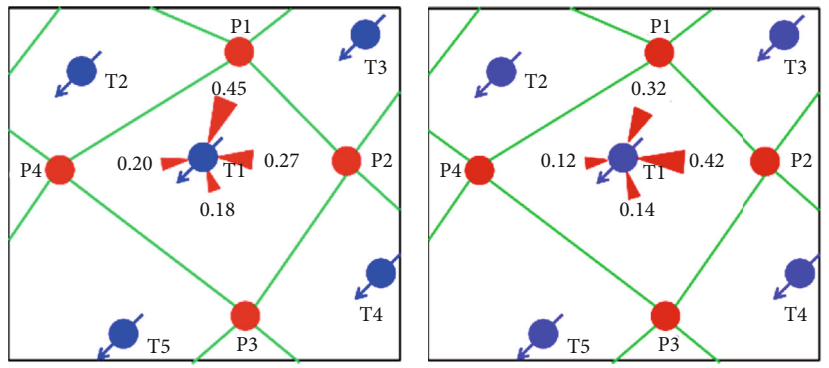

(a) Sandstone section

(b) Conglomerate section

Figure 17: The dividing coefficient diagram of the T1 well group.

Table 2: Tracer test results of the T1 well group.

Injector	Tracer type & inject date	Tracer well	Tracer breakthrough date	Tracer breakthrough time (day)	Tracer peak concentration (ng/ml)	Duration (day)
T1	Er 3/19/2019	P1	4/14/2019	26	148.66	41
		P2	5/11/2019	54	126.31	30
		P4	5/19/2019	62	97.04	36

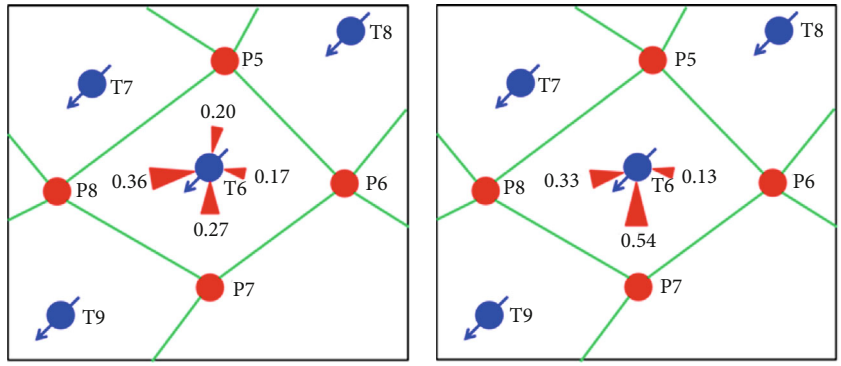

(a) Sandstone section (b) Conglomerate section

Figure 18: Dividing the coefficient diagram of the T6 well group.

Table 3: Tracer test results of the T6 well group.

Injector	Tracer type & inject date	Tracer well	Tracer breakthrough date	Tracer breakthrough time (day)	Tracer peak concentration (ng/ml)	Duration (day)
T6	Gd 3/20/2019	P8	5/9/2019	50	52.4	30
		P7	5/17/2019	58	97.01	26
	Sm 3/15/2019	P8	4/25/2019	41	82.41	21

As shown in Figure 14(b), the side of the channel bar is affected by river erosion. Locally inclined interlayers develop, which worsen the connectivity between wells. The water injection has a poor development, and substantial oil remains in this area. In the parallel source connectivity direction, when the interlayer distribution is more consistent with the source direction, the interwell connectivity is better, and the seepage channel is more developed. When the interlayer distribution is inconsistent with the source direction, the interwell connectivity is poor. In the vertical source direction connectivity, the interwell connection becomes poor due to the changes in the sand body contact relationships and permeability. There is no obvious dominant seepage channel in this area.

Based on the study of the remaining oil enrichment area and the connectivity characteristics of each layer, the A2 area in Figure 15 with higher remaining oil saturation and complex connection relationship is preferred as the adjustment area for the water injection efficiency evaluation. The water injection efficiency of injectors in A2 area is shown in Figure 16.

4.2. The Optimization of the Production System and Implementation Effect. Targeting the problem of dominant seepage channels in some directions of the well group in area A2 that caused the dividing coefficient to be concentrated, this study combined the automatic optimization method of the injector and producer working system to form three sets of adjustment plans.

The first plan is a liquid volume adjustment plan for water injection volume. Comparing the average water injection efficiency with the efficiency of different layers in different wells, there is an increase in water injection volume in the higher efficiency layer and conversely, the injection is reduced. For the connected producers, calculating the change in injected water volume in each direction according to the dividing coefficient and summing all as the liquid volume adjustment of the producers. The second plan is a reservoir property adjustment plan. The measures include profile control for inefficient injectors, as well as sealing, backflow, and well function reassignment for strong connectivity, large dividing coefficient, high water cut producers.

To ensure accurate and effective measures, the dividing direction and tracer test data of key well groups were verified.

In Figure 17, the plane dividing coefficient of injector T1 shows that the producers P1 and P2 of the same well group are the main dividing directions, with 45% and 27% of injected water diverted on the sandstone section, respectively, and 32% and 42% on the conglomerate section, respectively. Table. 2 shows a good correspondence among the three wells; the tracer test data from the T1 well group shows that P1 has the longest sustained dose time (41 days) and the highest peak tracer concentration (148.66 ng/ml); P2 has a continuous tracer time of 30 days and the peak tracer concentration 126.31 ng/ml; no tracer reaction was seen in P3; P4 continued to be seen for 36 days, and the peak tracer concentration was 97.04 ng/ml.

The water injection efficiency of T1 in the sandstone section was 0.15, and the water injection efficiency of the conglomerate section was 0.07; the water injection efficiency in the sandstone section was higher than the average water injection efficiency. The injection volume of T1 in the sand and conglomerate sections changed to 4.2 m^3 and 7.5 m^3, respectively.

In Figure 18, the horizontal dividing coefficient of T6 shows that the producers, P7 and P8, in the same well group are the main dividing directions, with 36% and 27% of the injected water diverted in the sandstone section, and 33%

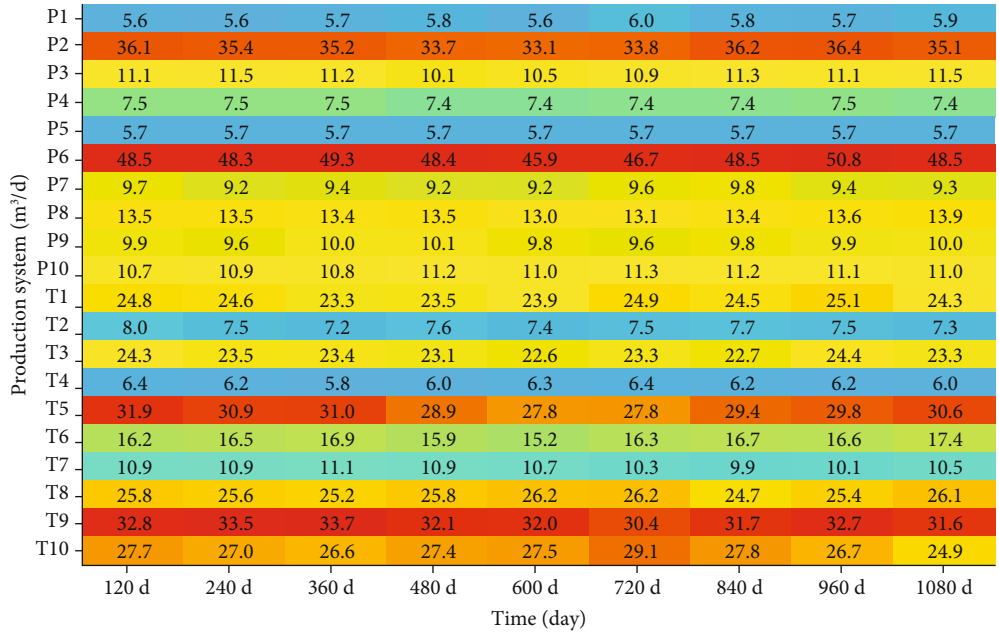

(a) Sandstone sections

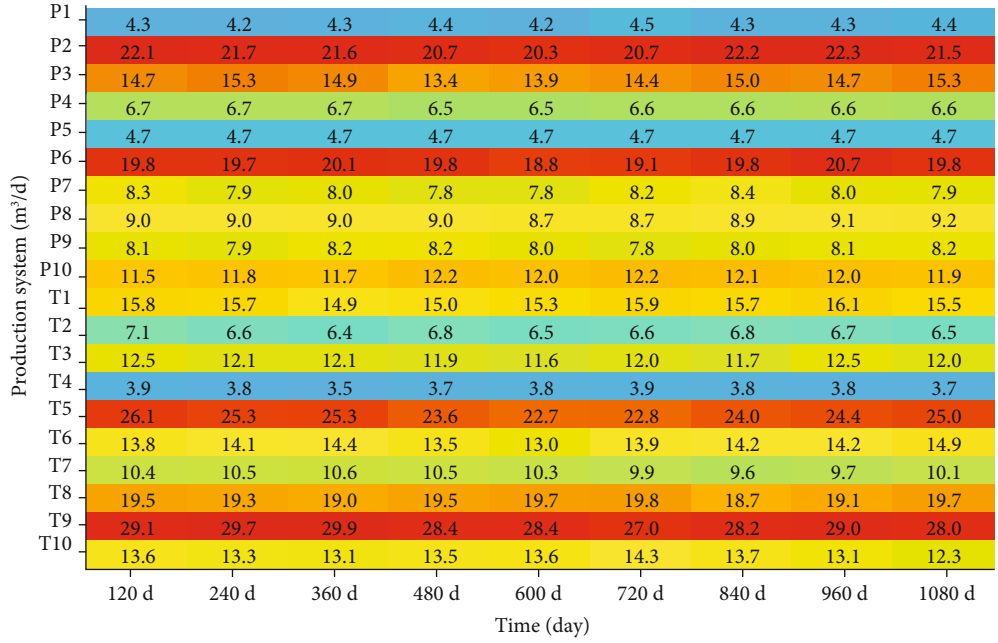

(b) Conglomerate sections

Figure 19: Adjusted production system.

and 54% in the conglomerate section, respectively. The tracer test data in Table 3 shows a good correspondence among the three wells. The tracer test data of the T6 well group shows that P7 lasted 26 days, and the peak tracer concentration was the highest (97.01 ng/ml). Two kinds of tracers were seen in P8, and the peak tracer concentrations were 52.4 ng/ml and 82.41 ng/ml, while no tracer reaction was seen in P5 and P6.

The water injection efficiency of T6 in the sandstone section was 0.17, and the water injection efficiency of the conglomerate section was 0.13. The water injection efficiency in both was higher than the average water injection efficiency. The injection fluid volume of the T6 increased to 5.0 m^3 in the sandstone section and increased to 3.5 m^3 in the conglomerate section.

After a three-year production simulation of the adjusted production system in Figure 19 and with comparisons to the original system, the daily oil production in the field increased by 15.5%; the cumulative oil production in the field increased by 4.24×10^4 t; the comprehensive water cut decreased by 1.39%, and the effect of the adjustment is obviously shown in Figure 20.

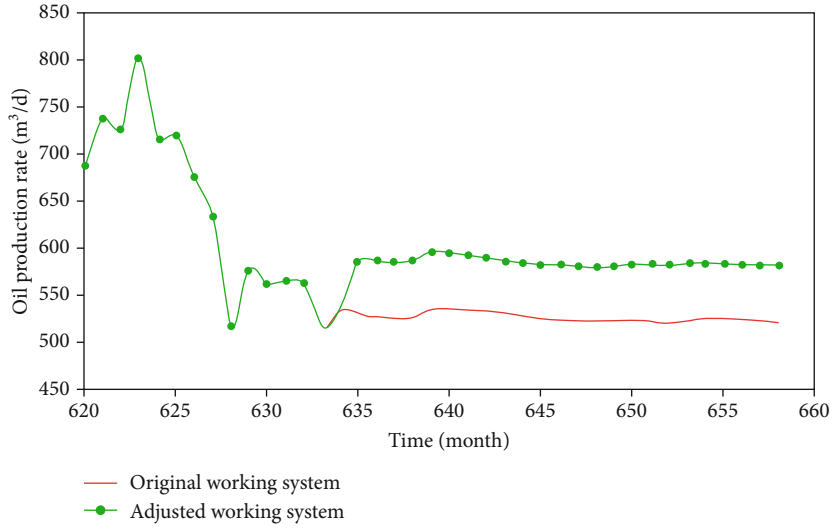

(a) Field daily oil production

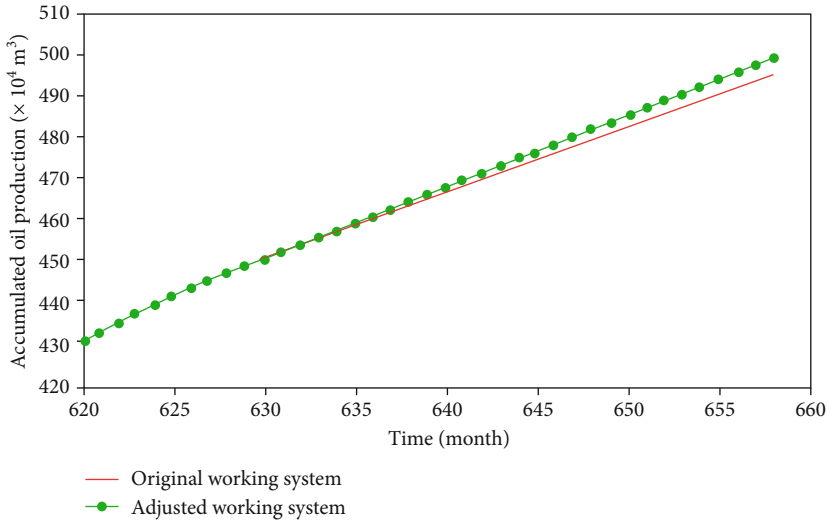

(b) Field cumulative oil production

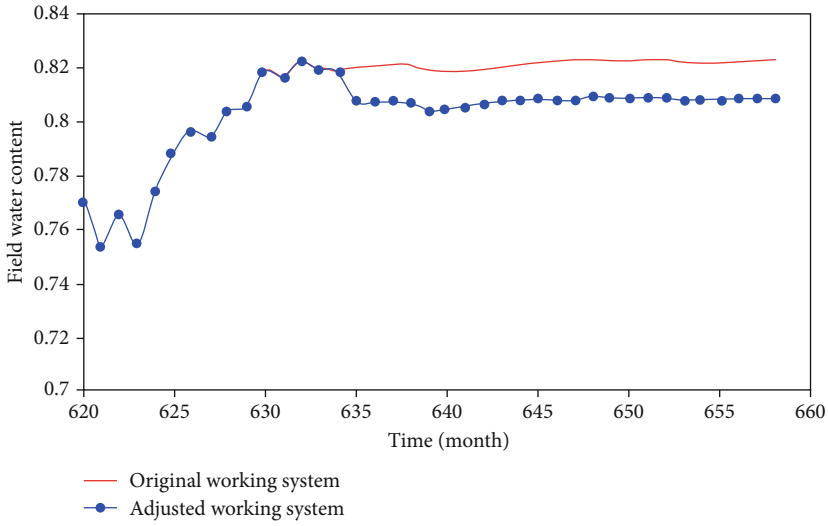

(c) Field water cut

Figure 20: The comparison of adjustment effect.

5. Conclusion

A layered water-injection efficiency evaluation method based on INSIM is proposed in this study by accurately adding virtual well points to characterize the actual geological connectivity of glutenite reservoirs and a well-to-well conductivity of the fitted connectivity model. Combined with the location of the sedimentary facies at the well point, a classification standard for interwell connectivity of glutenite was established, and the interwell connectivity was divided into four major categories and twelve subcategories. On this basis, to determine the injection water splitting quantity, the layered water injection efficiency of the injection well which is the basic knowledge to adjust the injection-production schedule was evaluated.

The method determines the vertical and horizontal water injection split coefficients by calculating data, such as connectivity parameters, pressure difference, and production index, and identifies the injection-production correspondence relationship and the effect of water injection. The calculation speed and the calculation result of the water injection efficiency are more reliable than the reservoir engineering method.

Based on this method, three types of liquid volume adjustment plans were formulated for an actual oilfield: injection-production structure adjustment, injection-production measurement adjustment, and comprehensive adjustment. It is predicted that after two years of implementation of the liquid volume adjustment measures for 20 water injection well groups in the A2 area, the daily oil production rate in the block will increase by 15.5%; the cumulative oil production in the block will increase by 4.24×10^4 t; the comprehensive water cut will decrease by 1.39%, and the effect of increasing oil precipitation will be obvious.

Nomenclature

A: Dividing coefficiency
b: Feature parameter matrix
b_r: Initial estimation of feature parameter matrix
C_t: Total compressibility, MPa^{-1}
e: Water injection efficient
e_x: Average water injection efficient
f_w: Water cut
G_B: Covariance matrix of the model parameters
G_D: Initial estimation covariance matrix of the model parameters
$\bar{h}$: Average interwell reservoir thickness, m
$h(b)$: Initial numerical simulation observation values
J: Production index
K: Layer average permeability, $10^{-3}\,\mu m^2$
$\bar{K}$: Interwell average permeability, $10^{-3}\,\mu m^2$
K_r: Relative permeability, $10^{-3}\,\mu m^2$
k_{obs}: Observation values
L: Well spacing, m
N_l: Number of reservoir layers
N_{Ic}: Number of connected injectors
N_w: Number of connected wells
O: Objective function for history matching
p: Flowing bottom hole pressure, MPa
q: Production or injection volume, m^3
r: Wellbore radius, m
s: skin factor
S_w: Water saturation
T: Transmissibility, $m^3/d{\cdot}MPa^{-1}$
V: Pore volume, m^3
η: Liquid volume adjustment coefficient
λ: Mobility, $10^{-3}\,\mu m^2/(mPa{\cdot}s)$
μ: Viscosity, mPa·s

Subscripts

i: Well-node index
ij: Parameters between well i and well j
j: Well-node index
k: Layer index
max: Parameter maximum
min: Parameter minimum
o: Oil phase
w: Water phase

Superscript

N: Timestep.

Data Availability

Data is available on request.

Conflicts of Interest

The authors declare that they have no conflicts of interest.

Acknowledgments

This study is sponsored by the China Petroleum Science and Technology Major Project (No. 2016B-1106).

References

[1] L. Sun, X. Wu, W. Zhou, X. Li, and P. Han, "Technologies of enhancing oil recovery by chemical flooding in Daqing oilfield, NE China," *Petroleum Exploration and Development*, vol. 45, no. 4, pp. 673–684, 2018.

[2] H. N. Al-Saedi and R. E. Flori, "Enhanced oil recovery of low salinity water flooding in sandstone and the role of clay," *Petroleum Exploration and Development*, vol. 45, no. 5, pp. 927–931, 2018.

[3] A. A. Yousef, S. H. al-Saleh, A. al-Kaabi, and M. S. al-Jawfi, "Laboratory investigation of the impact of injection-water salinity and ionic content on oil recovery from carbonate reservoirs," *SPE Reservoir Evaluation & Engineering*, vol. 14, no. 5, pp. 578–593, 2013.

[4] S. E. Buckley and M. C. Leverett, "Mechanism of fluid displacement in sands," *Transactions of AIME*, vol. 146, no. 1, pp. 107–116, 2013.

[5] G. Sheng, H. Zhao, Y. Su et al., "An analytical model to couple gas storage and transport capacity in organic matter with non-circular pores," *Fuel*, vol. 268, article 117288, 2020.

[6] Y. Zhao, L. Zhang, Y. Xiong, Y. Zhou, Q. Liu, and D. Chen, "Pressure response and production performance for multi-fractured horizontal wells with complex seepage mechanism in box-shaped shale gas reservoir," *Journal of Natural Gas Science & Engineering*, vol. 32, pp. 66–80, 2016.

[7] Z. Deliang, Z. Liehui, G. Jingjing, Z. Yuhui, and Z. Yulong, "Research on the production performance of multistage fractured horizontal well in shale gas reservoir," *Journal of Natural Gas Science & Engineering*, vol. 26, pp. 279–289, 2015.

[8] R. Zhang, G. S. Li, and J. C. Guo, "Experimental research into fracture propagation of complex lithologies in fractured tight oil reservoirs," *Petroleum Science Bulletin*, vol. 1, no. 3, pp. 353–362, 2016.

[9] H. Yu, Z. Yang, T. Ma, Z. Lei, S. Cheng, and H. Chen, "The feasibility of asynchronous injection alternating production for multistage fractured horizontal wells in a tight oil reservoir," *Petroleum Science Bulletin*, vol. 3, no. 1, pp. 32–44, 2018.

[10] J. M. Fan, C. Wang, X. F. Qu, L. B. Cheng, and T. Xue, "Development and practice of water flooding huff-puff in tight oil horizontal well, Ordos Basin: a case study of Yanchang formation Chang 7 oil layer," *Acta Petrolei Sinica*, vol. 40, no. 6, pp. 706–715, 2019.

[11] Z. Meng, S. L. Yang, L. Wang, Z. Wang, and W. Han, "Investigation on numerical simulation of co_2 huff and puff in tight oil reservoirs," *Journal of Petrochemical Universities*, vol. 29, no. 6, pp. 39–42, 2016.

[12] R. P. Batycky, M. J. Blunt, and M. R. Thiele, "A 3D field-scale streamline-based reservoir simulator," *SPE Reservoir Engineering*, vol. 12, no. 4, pp. 246–254, 2013.

[13] R. O. Baker, F. Kuppe, S. Chugh, R. Bora, S. Stojanovic, and R. Batycky, "Full-field modeling using streamline-based simulation: four case studies," *SPE Journal*, vol. 5, no. 2, pp. 126–134, 2002.

[14] M. R. Thiele and R. P. Batycky, "Using streamline-derived injection efficiencies for improved waterflood management," *Society of Petroleum Engineers*, vol. 9, no. 2, pp. 187–196, 2013.

[15] H. Hoteit and A. Firoozabadi, "Numerical modeling of two-phase flow in heterogeneous permeable media with different capillarity pressures," *Advances in Water Resources*, vol. 31, no. 1, pp. 56–73, 2008.

[16] A. M. Yousef, P. H. Gentil, J. L. Jensen, and L. W. Lake, "A capacitance model to infer interwell connectivity from production and injection rate fluctuation," *SPE Reservoir Evaluation & Engineering*, vol. 9, no. 6, pp. 630–646, 2013.

[17] M. Sayarpour, C. S. Kabir, and L. W. Lake, "Field applications of capacitance-resistance models in waterfloods," *SPE Reservoir Engineering*, vol. 12, pp. 853–864, 2009.

[18] D. Weber, T. F. Edgar, L. Lake, L. S. Lasdon, S. Kawas, and M. Sayarpour, "Improvements in capacitance-resistive modeling and optimization of large scale reservoirs," in *SPE Western Regional Meeting*, pp. 369–385, San Jose, CA, USA, 2009.

[19] A. Shabani, H. R. Jahangiri, and A. Shahrabadi, "Data-driven approach for evaluation of formation damage during the injection process," *Journal of Petroleum Exploration and Production Technology*, vol. 10, no. 2, pp. 699–710, 2020.

[20] H. Zhao, Z. Kang, X. Zhang, H. Sun, L. Cao, and A. C. Reynolds, "INSIM: a data-driven model for history matching and prediction for waterflooding monitoring and management with a field application," in *SPE Reservoir Simulation Symposium, vol. 1*, pp. 431–461, Houston, TX, USA, 2015.

[21] Z. Guo, A. C. Reynolds, and H. Zhao, "Waterflooding optimization with the INSIM-FT data-driven model," *Computational Geosciences*, vol. 22, no. 3, pp. 745–761, 2018.

[22] Z. Guo and A. C. Reynolds, "INSIM-FT in three-dimensions with gravity," *Journal of Computational Physics*, vol. 380, pp. 143–169, 2019.

[23] H. Zhao, L. Xu, Z. Guo, Q. Zhang, W. Liu, and X. Kang, "Flow-path tracking strategy in a data-driven interwell numerical simulation model for waterflooding history matching and performance prediction with infill wells," *SPE Journal*, vol. 25, no. 2, pp. 1007–1025, 2020.

[24] H. Zhao, L. Xu, Z. Guo et al., "A new and fast waterflooding optimization workflow based on INSIM-derived injection efficiency with a field application," *Journal of Petroleum Science and Engineering*, vol. 179, pp. 1186–1200, 2019.

[25] G. Sheng, Y. Su, and W. Wang, "A new fractal approach for describing induced-fracture porosity/permeability/ compressibility in stimulated unconventional reservoirs," *Journal of Petroleum Science and Engineering*, vol. 179, pp. 855–866, 2019.

[26] M. Thiele and R. Batycky, "Water injection optimization using a streamline-based workflow," in *SPE Annual Technical Conference and Exhibition*, pp. 521–526, Denver, CO, USA, 2003.

[27] L. Zhang, Y. Zhou, L. Zhao, and D. Zhang, "Finite element method using a characteristic-based split for numerical simulation of a carbonate fracture-cave reservoir," *Journal of Chemistry*, vol. 2015, Article ID 815051, 13 pages, 2015.